Nanoscale

ROYAL SOCIETY OF CHEMISTRY

COMMUNICATION

View Article Online
View Journal | View Issue

Check for updates

Cite this: *Nanoscale*, 2020, **12**, 2961

Received 10th December 2019,
Accepted 14th January 2020

DOI: 10.1039/c9nr10450j

rsc.li/nanoscale

Open Access Article. Published on 15 January 2020. Downloaded on 6/10/2026 10:23:49 PM.
This article is licensed under a Creative Commons Attribution 3.0 Unported Licence.

High resolution noncontact atomic force microscopy imaging with oxygen-terminated copper tips at 78 K†

Damla Yesilpinar, Bertram Schulze Lammers, Alexander Timmer, Saeed Amirjalayer, Harald Fuchs and Harry Mönig *

Functionalizing atomic force microscopy (AFM) tips by picking up single inert probe particles like CO or Xe from the surface drastically increase the resolution. In particular, this approach allows imaging organic molecules with submolecular resolution revealing their internal bonding structure. However, due to the weak coupling of these probe particles to both, the surface they are picked up from and the tip apex, these experiments require liquid helium temperatures (*i.e.* ≈5 K). In the present study we demonstrate that functionalizing an AFM tip with an atomically defined O-terminated copper tip (CuOx tip) allows performing such experiments at liquid nitrogen temperatures (*i.e.* ≈78 K) with outstanding quality. We show that it is possible to utilize CuOx tips for chemically selective imaging of a copper oxide nanodomain on a partially oxidized Cu(110) surface in the repulsive force regime at elevated temperatures. Moreover, the high structural and chemical stability of CuOx tips allow even *ex situ* investigations where these tips are used to perform experiments on other, non-Cu, non-oxidized, substrates. In particular, we present results obtained from a dicoronylene (DCLN) molecule with submolecular resolution. An analysis of inner and peripheral bond lengths of the DCLN molecule shows excellent agreement with theoretical gas phase simulations emphasizing the exceptional imaging properties of CuOx tips also at elevated temperatures.

The imaging mechanisms in scanning probe microscopy strongly depend on the chemical identity of the terminal atom of the probe tip.[1–5] Therefore, gaining control over the atomic configuration at the tip apex is one of the major challenges to ensure a reproducible and standardised data acquisition in such experiments. In particular, this constitutes a crucial step toward chemically selective imaging of surfaces with ultrahigh resolution.

In 2009, Gross *et al.*[6] demonstrated non-contact atomic force microscopy (NC-AFM) experiments where a metallic tip was functionalized by picking up a single CO molecule from the surface under study, which led to a chemical passivation of the apex. Furthermore, they used a tuning fork based force sensor in the qPlus configuration allowing for oscillation amplitudes well below 1 Å.[6,7] Both, the passivation of the tip termination and the small oscillation amplitudes facilitated NC-AFM imaging at reduced tip–sample distances where repulsive forces dominate the imaging contrast. They obtained a drastically increased resolution allowing to resolve the internal bonding structure of an adsorbed organic molecule.[6] There have also been attempts to pick up other (so called) probe particles from the surfaces for such experiments (*e.g.* Xe, Br, N_2O).[3,8–10] However, the majority of the research so far focused on CO-functionalized tips leading to a number of exceptional results in the last years.[6,7,9,11–16] A major drawback of the probe particle approach is related to the weak interconnection of the probe particles to the metallic apex. It has been shown that this leads to a pronounced lateral deflection of the probe particles at the apex during scanning, which results in image distortions and a considerable systematic overestimation of bond lengths in such experiments.[11,17] Moreover, this tip deflection can result in spurious bond-like contrast features at sites with strongly varying tip–sample potential.[18,19] Importantly, the weak coupling between the terminal particle and the metal apex (especially for CO and Xe) implies that such experiments can only be conducted at liquid helium temperatures (*i.e.* at ≈5 K). Higher temperatures would lead to instabilities or their desorption from the apex or surface. Thus far, NC-AFM imaging *via* qPlus sensors at elevated temperatures have been acquired either with undefined tip terminations and reduced imaging quality,[20] or with larger organic molecules attached to the metal tip, which need extensive calculations to confirm the probe particle configuration and exhibit complex tip flexibility effects.[21,22]

Recently, we established an alternative approach of tip functionalization involving a copper oxide tip termination for

Physikalisches Institut, Westfälische Wilhelms-Universität, Wilhelm-Klemm-Straße 10, 48149 Münster, Germany. E-mail: harry.moenig@uni-muenster.de

†Electronic supplementary information (ESI) available. See DOI: 10.1039/C9NR10450J

Open Access Article. Published on 15 January 2020. Downloaded on 6/10/2026 10:23:49 PM.
This article is licensed under a Creative Commons Attribution 3.0 Unported Licence.

submolecular imaging.[4,19,23–25] In particular, by slightly indenting a NC-AFM tip to a partially oxidized Cu(110) surface and subsequent contrast analysis above one of the typical copper oxide nanodomains (Fig. 1a and b) allows verifying an O-terminated copper tip (CuOx tip). As shown in Fig. 1a, a CuOx tip termination consists of a terminal single O atom, which is covalently connected in a tetrahedral configuration to the upper copper atoms of the tip. This tip is not only chemically inert, but also structurally considerably more stable than for example CO or Xe tips allowing to reduce the above mentioned imaging artefacts.[4,19,23]

In the present study we show high resolution NC-AFM imaging with experimentally verified CuOx-functionalized tips at ≈78 K (*i.e.* liquid nitrogen temperature). Extending the NC-AFM contrast analysis above a copper oxide nanodomain for CuOx tip identification to the repulsive force regime allows assessing tip asymmetry effects and excluding potential dimeric tips.[26] After successful functionalization, we show that, even at liquid nitrogen temperature, CuOx-tips are stable enough to endure sample exchange and therefore allow investigating a wide range of sample systems. Finally, after obtaining such an *ex situ* functionalized CuOx tip, we demonstrate tip-height dependent imaging of an organic molecule in the repulsive force regime with submolecular resolution. We found that the experimentally determined bond lengths from these data are in excellent agreement with theoretical values as derived from density functional theory (DFT) simulations.

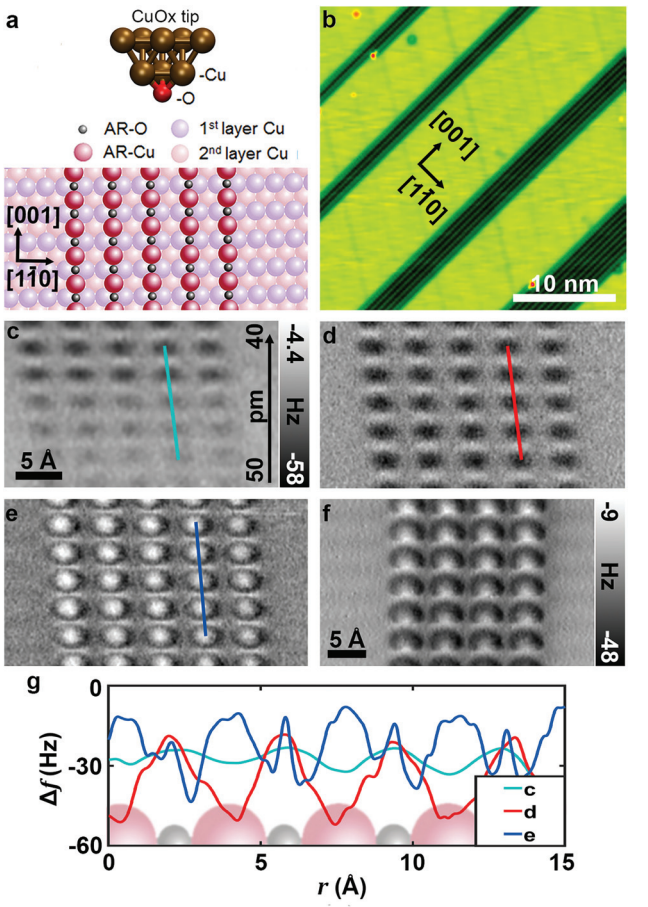

Fig. 1 (a) The models of the CuOx-tip and partially oxidized p(2 × 1)O–Cu(110) surface,[4] (b) STM image of the partially oxidized Cu surface used for tip preparation (V_{bias} = 100 mV, I_{set} = 20 pA), (c), (d) and (e) constant-height AFM images of one of the oxide stripes obtained with a symmetric CuOx-tip at LN_2 temperature at relative heights Δz_{ce} = 50 − 40 pm Δz_{de} = 40 pm (scale bar in c holds for the consecutive images) (f) constant-height AFM image on a typical oxide stripe obtained with an asymmetric CuOx-tip at 5 K (f_0 = 27 kHz; Q = 8846, A_{vib} ≈ 0.9 Å, U_{bias} = 0). (g) Line profile data obtained from marked region for each height (c–e).

The experiments were performed with a low-temperature scanning probe microscopy (SPM) system (ScientaOmicron, LT-STM/AFM) under UHV conditions at LN_2 temperature. A commercial quartz tuning fork cantilever in qPlus configuration[7] with electrochemically etched tungsten wire as a probe tip (f_0 = 27 kHz; Q = 854 at 78 K) was used to obtain both scanning tunneling microscopy (STM) and NC-AFM images. All STM images were recorded and the CuOx tip functionalization procedure was carried out at constant current feedback without tip oscillation. NC-AFM images were obtained by scanning the tip parallel to the surface at a determined height without feedback loop while the sensor was oscillated at an amplitude of ≈0.4 Å (U_{bias} = 0) unless specified otherwise. For *ex situ* investigations, 0.1 Langmuir DCLN molecule (gradient sublimed, >99.0% purity, obtained from Kentax) was evaporated at 643 K on a clean (non-oxidized) Cu(110) surface held at room temperature.

Fig. 1b shows an STM image of a partially oxidized Cu(110) surface. Dosing 0.2 Langmuir molecular oxygen at 450–500 K to this surface results in the typical (2 × 1)O-reconstructed oxide stripes along the [001] direction,[27] with a mean Cu stripe width of a few nanometers. As specified in Fig. 1a, the oxide stripes consist of single atomic chains of alternating Cu and O atoms. Although topographically higher, the oxide stripes appear as dark trenches in the STM image due to a reduced density of states above the oxide material. The procedures for obtaining an atomically defined CuOx tip termination on this surface has been described previously.[4,19] In brief, by using standard STM tip forming procedures, the electrochemically etched tungsten tips were covered with copper material by a combination of voltage pulses and indentations to the pure copper areas (bright stripes in Fig. 1b). Subsequently, the apex was repeatedly indented by a few Ångström into the oxide stripes to transfer copper oxide material to the tip. The successful formation of a CuOx tip termination can be confirmed by analyzing the NC-AFM contrast of an image recorded in constant frequency shift mode above one of the oxide stripes.[4] As shown by combined 3D force spectroscopy and DFT-based force–distance simulations, a CuOx tip termination can be verified when the copper atoms within the oxide are imaged as topographic maxima. Such a typical image can then serve as a unique fingerprint for a CuOx tip. In case of a negative or unclear contrast, further tip indentations were performed.

A recent study by Liebig *et al.*[26] about CuOx tip functionalization suggests that recording of a tip fingerprint image above

 This journal is © The Royal Society of Chemistry 2020

Open Access Article. Published on 15 January 2020. Downloaded on 6/10/2026 10:23:49 PM.
This article is licensed under a Creative Commons Attribution 3.0 Unported Licence.

an oxide stripe is considerably more reliable when it is taken in the repulsive force regime. Therefore, for our experiments at liquid nitrogen temperatures, we chose the constant-height NC-AFM mode for acquiring a tip fingerprint image to confirm a CuOx termination. To avoid extensive lateral and vertical tip–sample drift, we waited for about 3 to 4 hours until the feedback was switched off. At the beginning of the scan, z-drift was about ≈5 pm min^{-1} reducing the tip–sample distance over time. Fig. 1c shows a constant-height image recorded without z-drift correction allowing to assess the development of the contrast while the tip was drifting in during scanning. For Fig. 1d and e, z-drift was corrected during recording at the specific heights as indicated in the corresponding figure caption. Based on force–distance simulations, the minima and maxima in Fig. 1d clearly can be assigned to the copper and oxygen atoms within the oxide, respectively.[28] Upon entering the repulsive force regime (Fig. 1e), the oxide copper atoms are imaged with bright centers, while the oxygen atoms appear slightly less repulsive in between. The development of the line profiles at different tip heights shown in Fig. 1g demonstrates that the image in e (nominally z = 0 pm) is recorded in the regime where the repulsive forces dominate.

In general, the approach of tip indentation into the oxide stripes as described above, quite reliably leads to an oxygen terminated copper tip. However, experimentally it is somewhat demanding to obtain a CuOx tip where the terminal oxygen atom is oriented straight down. For CuOx tips where this is not the case, the copper atoms in the second layer of the tip can significantly contribute to the contrast, inducing a considerable asymmetry when imaging an organic molecule in the repulsive regime. Therefore, for our previous experiments performed at $T \approx 5$ K,[4,19,24,25,29] we usually co-adsorbed a low concentration of coronene molecules (≈0.05 Langmuir, corresponding to about 20 molecules on an area of 20 × 20 nm^2) on the partially oxidized Cu(110) surface.[29] This in turn helped to identify asymmetric tips in STM mode and to decide on continuing with further tip forming procedures. We have observed that the ease of obtaining a symmetric CuOx tip is correlated to the sharpness of the tip core of the qPlus sensor. With initially sharp tips, a symmetric CuOx-tip can be achieved with minimal effort. However, the process becomes laborious in the presence of blunt tips. Although deep indentations to the metallic surface help to restore a sharp tip apex, we have also found that resharpening these tips with focused ion beam (FIB) greatly reduces the time required for the tip functionalization procedure. In addition to tip asymmetry effects, it was demonstrated by Liebig *et al.*,[26] that the presence of two oxygen atoms at the apex can be identified by a pronounced asymmetry exclusively in the repulsive force regime. Whereas in the attractive force regime, the contrast of such a dimeric CuOx tip appears to have a perfectly symmetric apex. Upon entering the repulsive regime, these dimeric tips produce a distorted contrast as can be seen in Fig. 1f. Therefore, recording tip fingerprint images in the repulsive force regime allows for an unambiguous identification of atomically controlled, symmetric CuOx tips.

To demonstrate the broad applicability of CuOx NC-AFM imaging at reduced tip–sample distances (*i.e.* in the repulsive force regime) even at liquid nitrogen temperatures, we transferred the CuOx tip corresponding to the fingerprint images in Fig. 1c–e, to a different (non-oxidized) Cu(110) substrate with a ≈0.1 ML coverage of DCLN molecules (Fig. 2a). The sample was pre-cooled at the outer cryostat before insertion. The temperature inside the microscope initially rose up to 79.5 K following the sample exchange. After the exchange the Cu(110)/

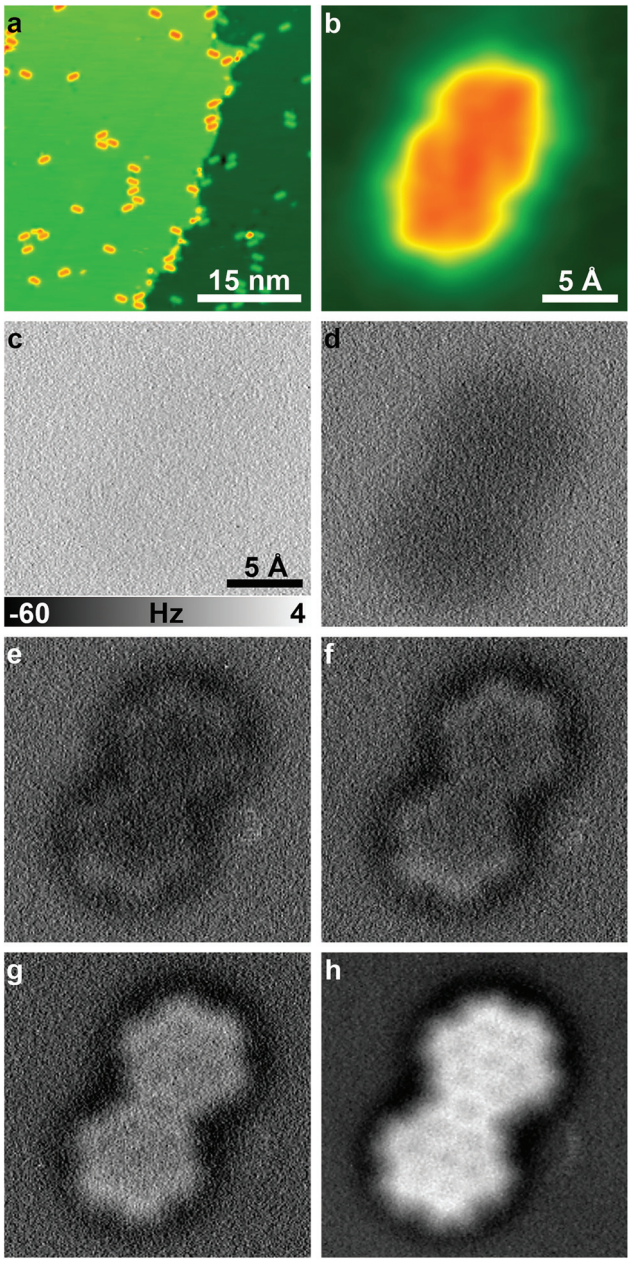

Fig. 2 (a) STM image of non-oxidized Cu(110) surface with ≈0.1 monolayer DCLN molecules. (b) STM image of the DCLN molecule taken before AFM experiments. Height dependent CH-AFM of DCLN molecule (c) at Δz_{ch} = 360 pm (d) at Δz_{dh} = 240 pm (e) at Δz_{eh} = 90 pm (f) at Δz_{fh} = 60 pm (g) at Δz_{gh} = 20 pm and (h) at the closest distance.

Open Access Article. Published on 15 January 2020. Downloaded on 6/10/2026 10:23:49 PM.
This article is licensed under a Creative Commons Attribution 3.0 Unported Licence.

DCLN sample was in cool-down position (microscope stage fully clamped to the liquid nitrogen bath cryostat) for ≈3 hours. Subsequently, the STM coarse approach of the tip was initiated at a piezo *z*-ramp speed of 40 nm s^{-1}, a bias voltage of −0.5 V, and a current set-point of 10 pA. After reaching tunneling contact, the tip was scanned on a 25 × 25 nm^2 area to ensure a reasonably defect-free region around the tip. To minimize lateral and vertical tip–sample drift effects, the tip was not moved for 12 hours overnight. The next morning the *x*/*y*-drift was ≈3–5 pm min^{-1}. Fig. 2b shows an STM image of a single DCLN molecule, which was then imaged by constant-height NC-AFM with the CuOx tip at various tip sample distances (Fig. 2c–h). During these measurements the *z*-drift (vertical drift) was slightly differing from image to image. While for the first and last image (Fig. 2c and h) a *z*-drift of ≈1 pm min^{-1} was compensated, during recording of the images in Fig. 2d–g there was hardly any vertical drift, and, therefore, those were recorded without any drift correction.

The series of constant-height NC-AFM images in Fig. 2c–h shows the development of the contrast in the raw data by reducing the tip sample distance by (in total) 360 pm where single steps are given in the figure caption. Submolecular resolution is achieved in Fig. 2e–h, clearly showing the bonding structure of the DCLN molecule. The level of structural detail in Fig. 2h can be further increased by applying Laplacian of Gaussian (LoG) filter to the data (Fig. 3a).

To further test the reliability of our data obtained at 78 K, we performed a comprehensive analysis of bond length from the data and compared the values from the experiment with DFT gas phase calculations for DCLN. The broad bond structure observed in the LoG filtered image proves challenging to obtain the experimental bond lengths with high accuracy, especially for peripheral bonds which are imaged broader compared to inner bonds. In order to sharpen the image contrast we used statistical difference (SD)[30] filter (Fig. 3b), and individually determined bond lengths for inner and peripheral bonds by fitting straight lines to the bonding structure (Fig. 3b and Fig. S2a†). The resulting averaged bond lengths per group of similar bonds highlighted in Fig. 3c and the calculated bond lengths for DCLN molecule are given on Table 1. Group

Table 1 Comparison of bond lengths acquired by CH-AFM and gas phase DFT calculations for DCLN molecule

Group	CH-AFM (Å)	DFT (Å)
A	1.38 ± 0.20	1.42
B	1.35 ± 0.20	1.37
C	1.51 ± 0.20	1.42
D	1.59 ± 0.20	1.47
E	1.30 ± 0.20	1.41
F	1.36 ± 0.20	1.38
G	1.47 ± 0.20	1.43
H	1.62 ± 0.20	1.42

A represents the bonds in the inner benzene rings, where the groups G and H cover the rest of the inner bonds, and the groups B–F are the peripheral bonds with different DFT-derived lengths.‡ Since the differences between the individual bond lengths are much lower than the uncertainty of our measurements, we grouped bonds according to their placement (peripheral bonds, inner benzene ring bonds and inner bonds) and then determined the subgroups according to DFT-derived values (*i.e.* bonds with similar values in DFT calculations were grouped together). The experimentally obtained values show excellent agreement with the calculated values for each group. The uncertainty of 0.20 Å in our measurements is comparable to reported uncertainty of 0.13 Å for CuOx tip measurements at LHe.[19] We also evaluated experimental line profiles to determine distances across opposite C–C bonds. The obtained values for all line profiles are found to be between 2.24 Å and 2.31 Å with an uncertainty of 0.25 Å.† Fig. 3d shows one typical line profile obtained from the line marked in Fig. 3a, with a width of 2.26 Å. The obtained values appear to be slightly underestimated, but still are well in the range of the experimental uncertainty as compared to the DFT-derived value of 2.47 Å.§ In agreement with the previous reports at LHe measurements with CuOx tips,[4,19] it is emphasized that a systematic overestimation of bond lengths as found in images obtained with flexible probe particles[11] is absent in our data.

In conclusion, we demonstrated controlled CuOx tip functionalization, tip characterization and imaging in constant-height mode in the repulsive force regime above a (2 × 1)

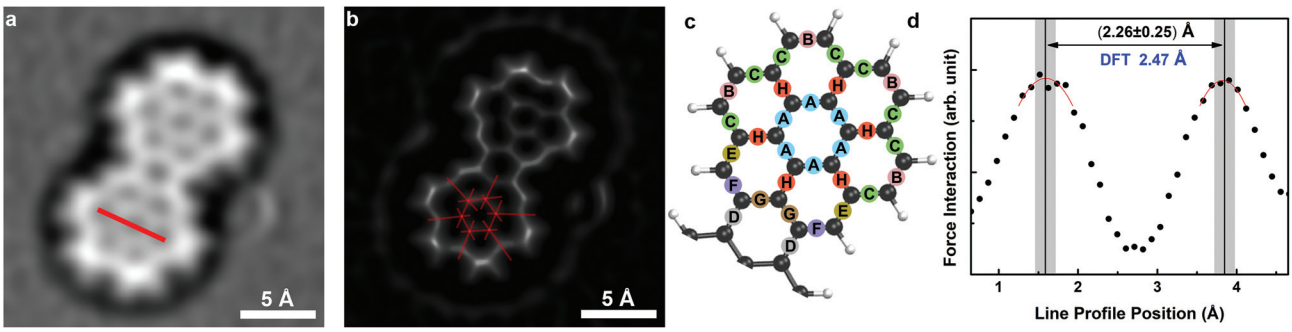

Fig. 3 (a) Image obtained at 78 K after LoG filter is applied, (b) SD filtered[30] image to sharpen the peripheral bonds for analysis, (c) the model showing half of the DCLN molecule, each letter representing a bond group according to their DFT lengths, (d) line profile obtained from LoG filtered image, marked by red line in (a).

This journal is © The Royal Society of Chemistry 2020

Open Access Article. Published on 15 January 2020. Downloaded on 6/10/2026 10:23:49 PM.
This article is licensed under a Creative Commons Attribution 3.0 Unported Licence.

O-reconstructed oxide stripe and an organic molecule on Cu (110) surfaces at liquid nitrogen temperatures (*i.e.* ≈78 K). The atomically defined tip termination in these experiments allows to clearly identify the chemical nature of the O- and Cu atoms within the imaged oxide. Therefore, our approach constitutes a considerable step toward chemical selective imaging of diverse atoms on a heterogeneous surface. Furthermore, the broad applicability of this experimental approach is emphasized by the possibility to allow sample exchange after controlled CuOx tip functionalization at increased temperatures. This was demonstrated by imaging an organic molecule adsorbed on a different, non-oxidized Cu(110) substrate (Fig. 2a) with submolecular resolution, clearly revealing its internal bonding structure with reasonable quality. The bond length investigations reveal a very good match with the DFT gas phase calculations, for both inner and peripheral bonds. We believe that the high structural and chemical stability of the CuOx tips qualifies our approach as a reliable solution to conduct high resolution NC-AFM imaging at elevated temperatures and bond length determination for organic species, across a wide variety of sample systems.

Conflicts of interest

There are no conflicts to declare.

Acknowledgements

This work was supported by the Deutsche Forschungsgemeinschaft through projects MO 2345/4-1, FU 299/19 and AM 460/2-1.

References

‡ The full version of the model DCLN molecule in Fig. 3c can be found on ESI.†
§ See ESI for more line profiles obtained from the image.†

1 R. Temirov, S. Soubatch, O. Neucheva, A. C. Lassise and F. S. Tautz, *New J. Phys.*, 2008, **10**, 053012.
2 N. Moll, L. Gross, F. Mohn, A. Curioni and G. Meyer, *New J. Phys.*, 2010, **12**, 125020.
3 F. Mohn, B. Schuler, L. Gross and G. Meyer, *Appl. Phys. Lett.*, 2013, **102**, 073109.
4 H. Mönig, D. R. Hermoso, O. Díaz Arado, M. Todorović, A. Timmer, S. Schüer, G. Langewisch, R. Pérez and H. Fuchs, *ACS Nano*, 2016, **10**, 1201.
5 X. Xin, L.-Y. Gan, M. A. Van Hove, X. Ren, H. Wang, C.-S. Guo and Y. Zhao, *ACS Omega*, 2016, **1**, 1004.
6 L. Gross, F. Mohn, N. Moll, P. Liljeroth and G. Meyer, *Science*, 2009, **325**, 1110.
7 F. J. Giessibl, *Rev. Sci. Instrum.*, 2019, **90**, 011101.
8 T. Chutora, B. de la Torre, P. Mutombo, J. Hellerstedt, J. Kopeček, P. Jelínek and M. Švec, *Beilstein J. Nanotechnol.*, 2019, **10**, 315.
9 L. Gross, B. Schuler, N. Pavliček, S. Fatayer, Z. Majzik, N. Moll, D. Peña and G. Meyer, *Angew. Chem., Int. Ed.*, 2018, **57**, 3888–3908.
10 P. Hapala, M. Švec, O. Stetsovych, N. J. van der Heijden, M. Ondráček, J. van der Lit, P. Mutombo, I. Swart and P. Jelínek, *Nat. Commun.*, 2016, **7**, 11560.
11 L. Gross, F. Mohn, N. Moll, B. Schuler, A. Criado, E. Guitián, D. Peña, A. Gourdon and G. Meyer, *Science*, 2012, **337**, 1326.
12 B. Schuler, W. Liu, A. Tkatchenko, N. Moll, G. Meyer, A. Mistry, D. Fox and L. Gross, *Phys. Rev. Lett.*, 2013, **111**, 106103.
13 S. P. Jarvis, *Int. J. Mol. Sci.*, 2015, **16**, 19936–19959.
14 D. G. de Oteyza, P. Gorman, Y.-C. Chen, S. Wickenburg, A. Riss, D. J. Mowbray, G. Etkin, Z. Pedramrazi, H.-Z. Tsai, A. Rubio, M. F. Crommie and F. R. Fischer, *Science*, 2013, **340**, 1434–1437.
15 L. Talirz, P. Ruffieux and R. Fasel, *Adv. Mater.*, 2016, **28**, 6222–6231.
16 S. Wickenburg, J. Lu, J. Lischner, H.-Z. Tsai, A. A. Omrani, A. Riss, C. Karrasch, A. Bradley, H. S. Jung, R. Khajeh, D. Wong, K. Watanabe, T. Taniguchi, A. Zettl, A. H. C. Neto, S. G. Louie and M. F. Crommie, *Nat. Commun.*, 2016, **7**, 13553.
17 S. Kawai, K. Takahashi, S. Ito, R. Pawlak, T. Meier, P. Spijker, F. F. Canova, J. Tracey, K. Nozaki, A. S. Foster and E. Meyer, *ACS Nano*, 2017, **11**, 8122.
18 P. Hapala, G. Kichin, C. Wagner, F. S. Tautz, R. Temirov and P. Jelínek, *Phys. Rev. B: Condens. Matter Mater. Phys.*, 2014, **90**, 085421.
19 H. Mönig, S. Amirjalayer, A. Timmer, Z. Hu, L. Liu, O. Díaz Arado, M. Cnudde, C. A. Strassert, W. Ji, M. Rohlfing and H. Fuchs, *Nat. Nanotechnol.*, 2018, **13**, 371.
20 F. Huber, S. Matencio, A. J. Weymouth, C. Ocal, E. Barrena and F. J. Giessibl, *Phys. Rev. Lett.*, 2015, **115**, 066101.
21 A. M. Sweetman, S. P. Jarvis, H. Sang, I. Lekkas, P. Rahe, Y. Wang, J. Wang, N. R. Champness, L. Kantorovich and P. Moriarty, *Nat. Commun.*, 2014, **5**, 3931.
22 A. M. Sweetman, S. P. Jarvis, P. Rahe, N. R. Champness, L. Kantorovich and P. Moriarty, *Phys. Rev. B: Condens. Matter Mater. Phys.*, 2014, **90**, 165425.
23 H. Mönig, *Chem. Commun.*, 2018, **54**, 9874.
24 L. Liu, H. Klaasen, A. Timmer, H.-Y. Gao, D. Barton, H. Mönig, J. Neugebauer, H. Fuchs and A. Studer, *J. Am. Chem. Soc.*, 2018, **140**, 6000.
25 H.-Y. Gao, M. Šekutor, L. Liu, A. Timmer, H. Schreyer, H. Mönig, S. Amirjalayer, N. A. Fokina, A. Studer, P. R. Schreiner and H. Fuchs, *J. Am. Chem. Soc.*, 2019, **141**, 315.
26 A. Liebig and F. J. Giessibl, *Appl. Phys. Lett.*, 2019, **114**, 143103.
27 K. Kern, H. Niehus, A. Schatz, P. Zeppenfeld, J. Goerge and G. Comsa, *Phys. Rev. Lett.*, 1991, **67**, 855.
28 H. Mönig, M. Todorović, M. Z. Baykara, T. C. Schwendemann, L. Rodrigo, E. I. Altman, R. Pérez and U. D. Schwarz, *ACS Nano*, 2013, **7**, 10233.
29 A. Timmer, H. Mönig, M. Uphoff, O. Díaz Arado, S. Amirjalayer and H. Fuchs, *Nano Lett.*, 2018, **18**, 4123.
30 SPIP V5.1.11 Scanning probe image processor (Hørsholm: Image Metrology), https://www.imagemet.com/.